

UKAEA-CCFE-PR(23)168

K. Amjad, W.J.R. Christian, K. Dvurecenska, D.
Mollenhauer, C.P. Przybyla, E. A. Patterson

Quantitative Comparisons of Volumetric Datasets from Experiments and Computational Models

Enquiries about copyright and reproduction should in the first instance be addressed to the UKAEA Publications Officer, Culham Science Centre, Building K1/O/83 Abingdon, Oxfordshire, OX14 3DB, UK. The United Kingdom Atomic Energy Authority is the copyright holder.

The contents of this document and all other UKAEA Preprints, Reports and Conference Papers are available to view online free at scientific-publications.ukaea.uk/

Quantitative Comparisons of Volumetric Datasets from Experiments and Computational Models

K. Amjad, W.J.R. Christian, K. Dvurecenska, D. Mollenhauer, C.P.
Przybyla, E. A. Patterson

Date of publication xxxx 00, 0000, date of current version xxxx 00, 0000.

Digital Object Identifier 10.1109/ACCESS.2022.Doi Number

Quantitative Comparisons of Volumetric Datasets from Experiments and Computational Models

K. Amjad^{1,2}, W.J.R. Christian¹, K. Dvurecenska¹, D. Mollenhauer³, C.P. Przybyla³ and E. A. Patterson¹

¹School of Engineering, University of Liverpool, Liverpool, UK

²United Kingdom Atomic Energy Authority, Culham Science Centre, Abingdon, UK

³Air Force Research Laboratory, Materials & Manufacturing Directorate, Wright-Patterson AFB, Ohio, USA

Corresponding author: K. Amjad (e-mail: amjadk@liverpool.ac.uk).

This work was sponsored by the Air Force Office of Scientific Research, Air Force Material Command, USAF under grant number FA9550-17-1-0272. The U.S. Government is authorised to reproduce and distribute reprints of Governmental purpose notwithstanding any copyright notation thereon. Lt. Col. Dave Garner (EOARD) and Dr Jaimie S Tiley (AFOSR) were the program officers for this grant.

ABSTRACT Wide-spread availability of low-cost digital sensors has made the acquisition of full-field experimental measurements less challenging, with modern measurement systems capable of obtaining three dimensional (3D) data fields. This presents difficulties when comparing computational and corresponding experimental data that often do not share the same orientation, scale, coordinate system or data pitch. This paper presents a method for performing quantitative comparisons of 3D data fields, irrespective of the source from which they are acquired. Two case-studies, each involving a pair of computational and experimental datasets, were used in this paper to demonstrate the capability of the method. The first case study represented the internal 3D strain fields in a reinforced-rubber matrix specimen under tensile load, measured using digital volume correlation, whilst the second study involved time-varying, surface displacements of an aerospace panel under resonance, which were measured using digital image correlation. The proposed orthogonal decomposition-based method works by representing 3D datasets as feature vectors, thereby allowing one-to-one comparison of the datasets within the feature vector space regardless of whether the original datasets share the same coordinate system, scale or data pitch.

INDEX TERMS image decomposition, digital images, volume measurement, pattern matching, finite element analysis, data correlation, model validation

I. INTRODUCTION

The emergence of relatively low-cost digital sensors has revolutionized experimental measurements by allowing information-rich data fields to be acquired in real-time, in a wide range of environments with adjustable spatial and temporal resolutions. The relative ease of acquiring information-rich data from full-field measurement techniques has allowed researchers to make significant advances over the last two decades in the areas of data fusion in both non-destructive evaluation [1] and finite element (FE) model updating [2]. Moreover, there has been a paradigm shift in the design and life cycle management processes for large-scale structures. Integrated digital environments are being developed to link computational data from multi-physics and

multi-scale simulations to experimental data from full-field and point sensors to cut down operational and maintenance costs and reduce conservatism in traditional design standards, whilst maintaining the highest standards of safety and reliability. In this context, a major computational challenge which researchers have faced is the difficulty in comparing datasets from different experimental and computational sources containing thousands of point values that often do not share the same orientation, scale, coordinate system or data pitch.

A predominant approach to comparison of full-field datasets in industry and academia still relies on visual similarity between datasets, which is qualitatively established by visualizing the datasets using colour maps [3], line profiles

TABLE 1
Limitations and strengths of key existing methods for full-field data comparison (with exemplar references).

Methods for full-field data comparison	Limitations	Strengths
Visual comparison based on colour maps [3]	<ul style="list-style-type: none"> Limited primarily to 2D datasets Does not provide any quantitative measure of the difference or agreement. 	<ul style="list-style-type: none"> Easy-to-implement method for identifying obvious visual differences; often used as a first step in preliminary data comparison.
Visual comparison based on scatter plot [5], [6]	<ul style="list-style-type: none"> Coefficient of determination and slope of the best-fit line are considered as partial measures of correlation between two datasets. Does not provide information about localized differences in 2D and 3D data arrays. 	<ul style="list-style-type: none"> Easy-to-implement; considered as a first step towards quantitative data comparison
Comparison of DIC and FE data [22]	<ul style="list-style-type: none"> Specific to comparison between 2D datasets from DIC and FE models 	<ul style="list-style-type: none"> Allows one-to-one quantitative comparison of 2D datasets in physical measurement space
Quantitative comparison of two volumetric datasets [23]	<ul style="list-style-type: none"> Basis vectors for datasets not identical which does not allow strict one-to-one comparison 	<ul style="list-style-type: none"> Allows quantitative comparison of 3D datasets in spectral space.

[4] or scatter plots [5], [6]. For instance, Zauel *et al.* [5] established similarity between FE model predictions and digital volume correlation (DVC) measurements of internal three-dimensional (3D) deformation fields in human cancellous bone under load by applying linear regression to the scatter plot of FE and experiment data points and evaluating the coefficient of determination and slope of the best-fit line. More recently, Oliviero *et al.* [6] used an identical approach to validate FE predictions of deformation fields in mouse tibia bone under compression with DVC measurements. Germaneau *et al.* [3] used colour maps for qualitative comparison of FE-predicted displacements fields of a spherical plane bearing with DVC measurements, whereas Ksvayee *et al.* [4] utilized line plots to compare the strain distribution in a ductile iron microstructure predicted using FE with digital image correlation (DIC) measurements.

In general, a more quantitative analysis of large datasets involves discovering the dominant patterns or features in the raw data by employing feature extraction methods [7]. Proper orthogonal decomposition, which is also referred to as principal component analysis (PCA) depending on the field of application, is one of the most common approaches to feature extraction used by researchers to analyze large amounts of experimental data [8], [9]. PCA is mainly based on the mathematical technique of matrix diagonalization, or more specifically, singular value decomposition. It linearly transforms or decomposes the original dataset into an optimal set of basis vectors thereby giving singular values or principal components which represent the most significant features of the original data. PCA is predominantly used in the fields of fluid mechanics and structural dynamics to study complex flow fields [10], [11] and the dynamic response of structures [12], [13], respectively. The use of PCA has also been explored in the optimization of manufacturing process parameters of automobile parts [14]. In the past decade, an image decomposition method based on discrete orthogonal polynomials [15], [16], [17] has gained popularity in the field

of experimental solid mechanics. In this method, surface deformation fields of displacement, stress or strain, acquired from optical techniques such as DIC, electronic speckle pattern interferometry (ESPI) or thermoelastic stress analysis (TSA), are treated as digital images and subsequently decomposed using a set of pre-defined two-dimensional (2D) shape descriptors or kernels, which are formed from one-dimensional (1D) discrete orthogonal polynomials. The coefficients of the fitted kernels are collated into a vector. This vector, which is referred to as a feature vector, provides a unique and accurate representation of the original data, but typically using less than a hundred coefficients instead of $>10^3$ data values. These feature vectors allow one-to-one comparison of the data fields within the feature vector space regardless of whether the original data fields share the same coordinate system, scale or data pitch. This one-to-one comparison is usually not possible with PCA since it essentially transforms the original dataset into an optimal set of basis vectors, which are not necessarily the same for the given datasets to be compared. The development of the image-based orthogonal decomposition method has led to new approaches for finite element (FE) model updating [16] and quantitative validation of computational mechanics models [18], [19] using displacement or strain fields on the surface of structures. The Euclidean distance between feature vectors describing the strain fields has also been used to develop novel approaches for detecting and monitoring damage in both metallic [20] and composite [21] components.

Alternate methods to orthogonal decomposition have also been proposed for quantitative comparison of full-field datasets from different sources [22], [23]. However, these methods are either suited to a specific source of dataset [22] or are encountered with similar issues to PCA where the basis vectors are not necessarily identical for the given datasets to allow one-to-one comparison in the feature space [23]. For instance, Lava *et al.* [22] proposed a framework for quantitative validation of FE data using DIC. In this method,

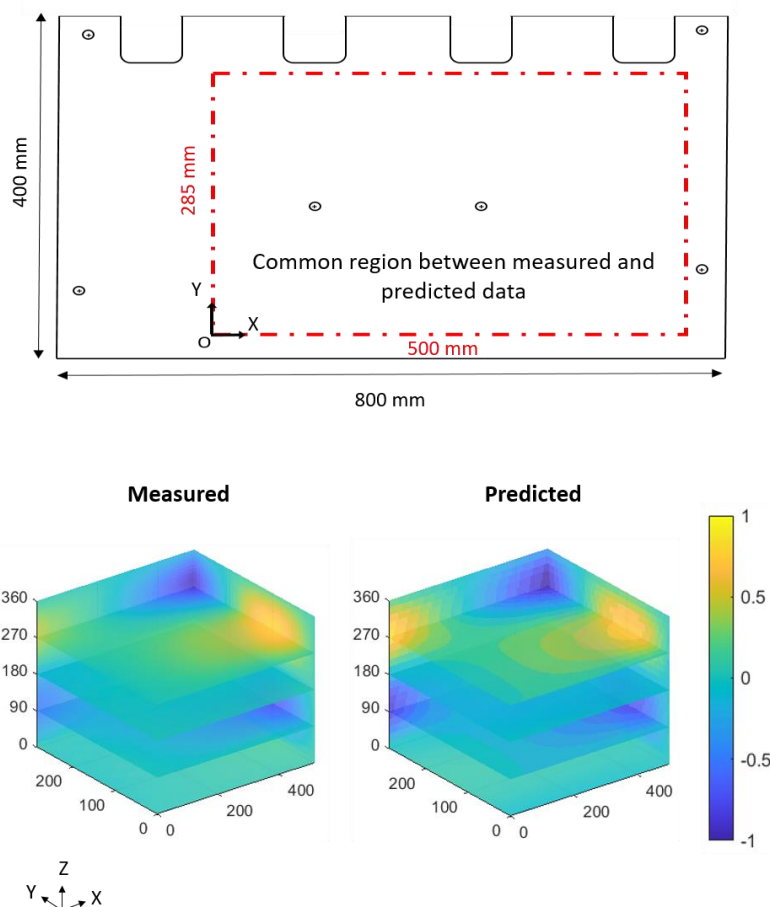


FIGURE 1. Schematic of the aerospace panel (top) and the volumetric arrays (bottom) constructed from measured (left) and predicted (right) out-of-plane displacement data over the common region of interest. This figure is best interpreted in colour.

FE-predicted displacement fields are used to numerically deform the digital images of the speckle pattern, which was created on the specimen's surface for DIC measurements. The sets of numerically-deformed and original images are then processed separately using the same DIC algorithm for strain measurements. The resulting FE-based and the experimental DIC-based strain fields, by default, shared the same grid size and data pitch for one-to-one comparison. Salloum *et al.* [23] proposed a method based on Alpert multi-wavelets capable of decomposing both 2D and 3D datasets into spectral space. However, their decomposition approach does not result in identical basis vectors for given datasets and thus slight inconsistencies in the basis vector directions do not allow for one-to-one comparison of the datasets in the feature space. The strengths and the limitations of the key existing methods for full-field data comparisons, discussed above, are summarized in Table 1.

This paper extends the image-based orthogonal decomposition method to three dimensions. This allows any volumetric data array to be orthogonally decomposed and uniquely described as feature vectors using a predefined set of basis vectors, and hence, addresses the major limitations of the

previously published methods listed in Table 1. Major sources of volumetric datasets include tomography [24], [25] and serial sectioning [26] techniques, which are used extensively for determining the internal 3D structure of components. The proposed volume decomposition algorithm is equally capable of decomposing temporally-varying 2D fields of data, which are typically acquired from techniques such as high-speed DIC [27] and infra-red thermography [28]. The proposed algorithm decomposes the volumetric data arrays into feature vectors in exactly the same manner as the image decomposition method does for the 2D data fields. It is, therefore, envisaged that the methodologies [19], [29] developed for quantitative comparison of 2D data fields in feature vector space are applicable to volumetric datasets as well. Hence, one of the objectives of this paper is to establish the applicability of these quantitative comparison methodologies to volumetric datasets by employing the proposed volume decomposition algorithm.

This paper is structured in the following manner: the next section (Sect. II) describes the orthogonal decomposition algorithm for volumetric datasets. Two pairs of measured and predicted datasets were analyzed in this study, which are described in Sect. III. The process of decomposing a

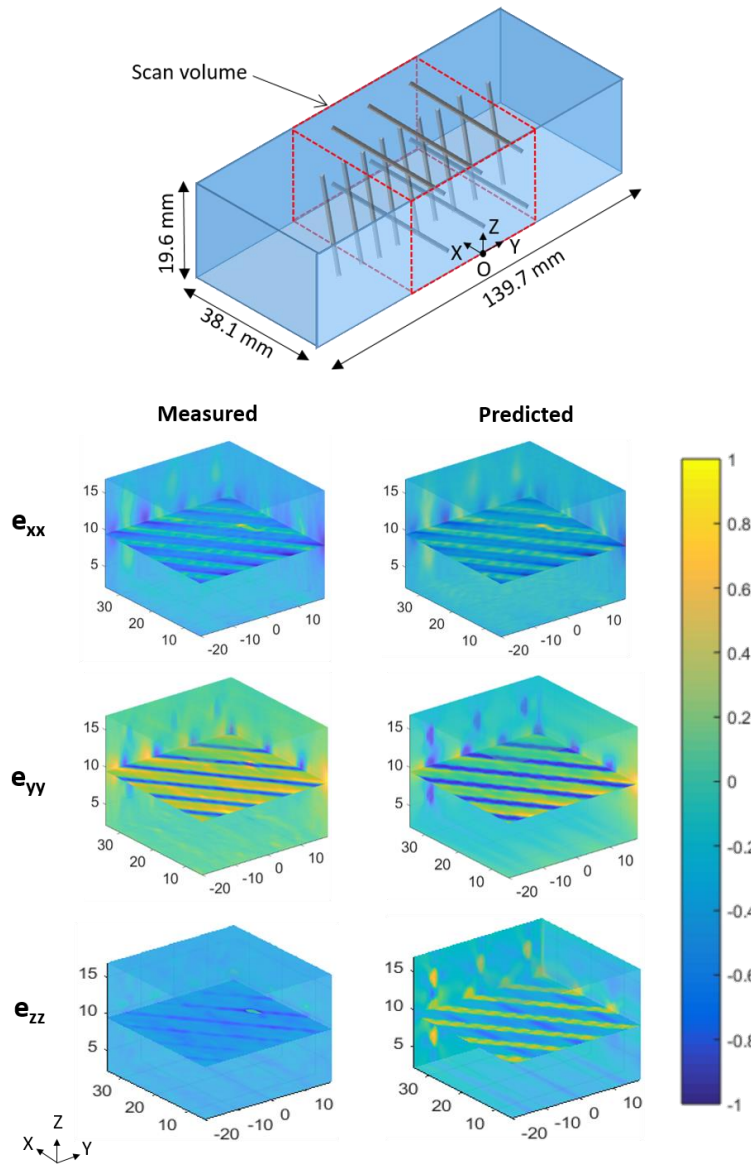


FIGURE 2. Schematic of the reinforced-rubber matrix specimen (top) and the volumetric arrays of measured (left) and predicted (right) data. This figure is best interpreted in colour

volumetric array into its feature vector is described in Sect. IV using experimentally measured data arrays. In Sect. V, FE model validation is performed by quantitatively comparing the FE-predicted volumetric arrays with the experimentally measured ones after transforming them into feature vectors. The results are discussed in Sect. VI with concluding remarks provided in Sect. VII. Data on which this study is based was analyzed using Matlab (version: R2020a) and can be accessed from Dryad Digital Repository at: http://datadryad.org/stash/share/TWpuPHB9jpk2aEIR84xxJRwszTdjT_MDUj-ID1xymCY

II. Orthogonal volume decomposition algorithm

3D kernel functions are required to decompose a 3D array of data. These kernels are formed from 1D Chebyshev polynomials, which are defined using the recursive formula [15]:

$$t_k(a) = \frac{(2k-1)t_1(a)t_{k-1}(a) - (k-1)\left(1 - \frac{(k-1)^2}{K^2}\right)t_{k-2}(a)}{k}, \quad k = 2, 3, \dots, K-1 \quad (1)$$

$$t_0(a) = 1 \quad (2)$$

$$t_1(a) = \frac{2a+1-K}{K} \quad (3)$$

where k , is the order of the polynomial, K , is the number of sampling points and a is the sample location. These discrete

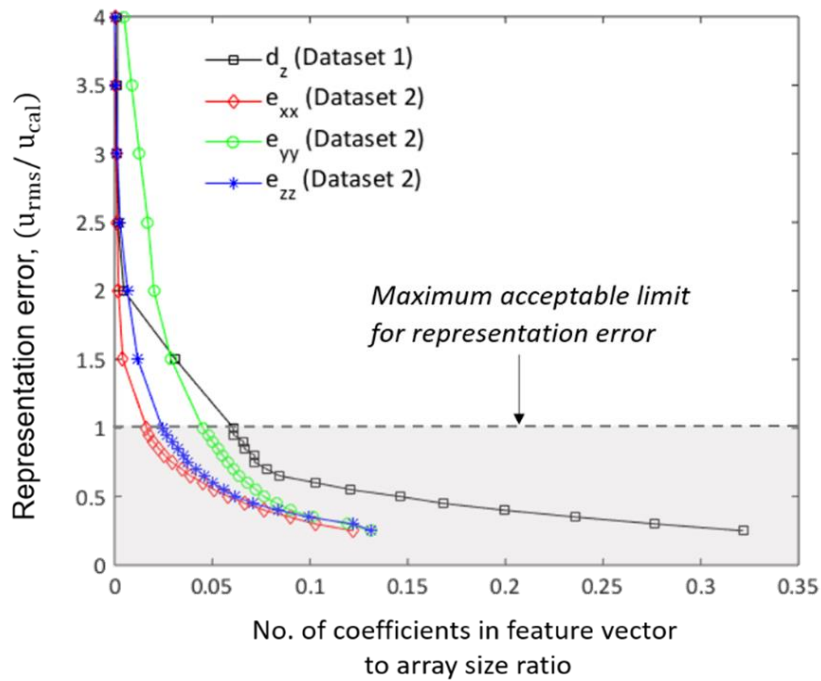


FIGURE 3. Plot showing the decrease in representation error, defined as a ratio of the minimum measurement uncertainty, with the increasing number of coefficients in unprocessed feature vectors, stated as a ratio of the data array size, for the four measured data arrays shown in Fig. 1 and 2. The array sizes for z-displacement in Dataset 1 (panel) and the three strain components in Dataset 2 (reinforced rubber matrix) are 1.18×10^5 and 7.78×10^5 , respectively. The shaded segment of the plot highlights those feature vectors with a representation error equal to or lower than u_{cal} .

polynomials can be combined to obtain three-dimensional orthogonal kernels, of dimensions $M \times N \times O$, using:

$$T_{m,n,o}(x, y, z) = t_m(x)t_n(y)t_o(z) \quad (4)$$

where m , n and o are the order of the 1D polynomials. When combined, the order of the 3D kernel is calculated as:

$$\omega_{m,n,o} = m + n + o \quad (5)$$

To use the orthogonal kernels for decomposition they must first be normalized by dividing each kernel by its associated norm. To obtain the norm with minimal computational errors it can be calculated analytically as:

$$\mathcal{P}_{m,n,o} = \rho_m \rho_n \rho_o \quad (6)$$

where [16]:

$$\rho_m = \frac{M(1-\frac{1}{M^2})(1-\frac{2^2}{M^2}) \dots (1-\frac{m^2}{M^2})}{2m+1} \quad (7)$$

The data array I can then be decomposed into coefficients, $T_{m,n,o}$, using:

$$T_{m,n,o} = \sum_{x,y,z=0}^{M,N,O} I(x, y, z) \frac{1}{\sqrt{MNO}} \frac{T_{m,n,o}(x,y,z)}{\sqrt{\mathcal{P}_{m,n,o}}} \quad (8)$$

The reconstruction of the data array is calculated as:

$$\hat{I}(x, y, z) = \sum_{m,n,o=0}^{M,N,O} T_{m,n,o} \sqrt{MNO} \frac{T_{m,n,o}(x,y,z)}{\sqrt{\mathcal{P}_{m,n,o}}} \quad (9)$$

The coefficients are arranged as a 3D array, these can be permuted using the ordering system described by Bateman [30] which has been extended here to three dimensions. Using this system, the coefficient $T_{m,n,o}$ comes before $T_{p,q,r}$ in the feature vector if either of the following conditions are true:

$$\omega_{m,n,o} < \omega_{p,q,r} \quad (10)$$

$$(\omega_{m,n,o} = \omega_{p,q,r}) \wedge (m + nN + oNO < p + qN + rNO) \quad (11)$$

where \wedge , is the mathematical notation for “logical and”. This results in a feature vector \mathbf{f} , ordered as follows:

$$\mathbf{f} = \left\{ \begin{array}{c} T_{0,0,0} \\ T_{1,0,0} \\ T_{0,1,0} \\ T_{0,0,1} \\ T_{2,0,0} \\ T_{1,1,0} \\ \vdots \\ T_{M-1,N-1,O-1} \end{array} \right\} \quad (12)$$

This permutation scheme ensures that the feature vector is ordered so that coefficients corresponding with the same order of 3D kernel appear together in the feature vector, with the order increasing when moving down the vector. The choice of

TABLE 2
Number of significant coefficients in the refined feature vectors with $u_{rms} \approx u_{cal}$ and the corresponding ratios of reduction in data size for the four measured arrays in the exemplar datasets.

Exemplar	Quantity of interest	Original data size	No. of significant coefficients in the refined feature vector with	Ratio of data size reduction
			$u_{rms} \approx u_{cal}$	
Panel	d_z	1.18×10^5	758	155 : 1
Reinforced rubber matrix	e_{xx}	7.78×10^5	2650	293 : 1
	e_{yy}	7.78×10^5	6867	113 : 1
	e_{zz}	7.78×10^5	6014	129 : 1

permutation scheme only affects where values appear within the vector, and any other scheme could be used resulting in no change to the findings of this study. The number of coefficients in the feature vector \mathbf{f} , when using all the kernels up to a maximum order of ω_{max} is a tetrahedral number, and thus can be calculated as:

$$\Omega = \frac{1}{6}\omega_{max}^3 + \omega_{max}^2 + \frac{11}{6}\omega_{max} + 1 \quad (13)$$

This equation has two imaginary roots and a single real root equal to the order of the polynomials required to populate a feature vector of any arbitrary length. For this study, the roots were found using the “roots” function built into Matlab, which works by calculating the eigenvalues of the companion matrix of equation (13).

A. Representation error

The representation error is the difference between the original data volume and its reconstruction. When reconstructing real-valued data, a common technique for quantifying the representation error is to use the root mean squared error, calculated as:

$$u_{rms} = \sqrt{\frac{1}{MNO} \sum_{x,y,z=0}^{M,N,O} (I(x,y,z) - \hat{I}(x,y,z))^2} \quad (14)$$

This measure can also be used for assessing the reconstruction of binary volumes of data. However, in this situation, the mean absolute error is more effective as it calculates the proportion of incorrect voxels in the reconstruction. The mean absolute error is given as:

$$u_{mae} = \frac{1}{MNO} \sum_{x,y,z=0}^{M,N,O} |I(x,y,z) - \hat{I}_{bin}(x,y,z)| \quad (15)$$

The feature vectors can be processed to minimize the number of non-zero coefficients by truncating them at a particular length or setting all coefficients to zero that have an absolute value less than a pre-specified threshold, i.e. filtering. When filtering a feature vector, it is necessary to calculate the representation error to assess whether additional filtering can be undertaken to further reduce the number of non-zero elements in the vector while satisfying requirements for the quality of the representation. This requires repetitive calculations using equations (9) and (14), greatly increasing the computation time. The kernels used to represent the data volume are orthogonal and thus the representation error can be

calculated without actually reconstructing the data using Parseval’s theorem as [30]:

$$u_{rms} = \sqrt{\frac{1}{MNO} \sum_{x,y,z=0}^{M,N,O} I(x,y,z)^2 - \sum_i \check{f}_i^2} \quad (16)$$

where $\check{\mathbf{f}}$ denotes the filtered feature vector. Using this equation, it is possible to decompose a volume into a feature vector containing a high number of coefficients and then rapidly determine the minimum number of coefficients required to just achieve an arbitrary representation error.

B. Decomposition using matrix operations

Decomposition and reconstruction using equations (8) and (9) are computationally-intensive tasks as they require many iterations and substantial amounts of computer memory. The computation of the coefficients can be performed more efficiently using matrix operations, which can be calculated using concurrent computation. If the data is considered as a 3D array, the z^{th} slice through the array $I_{x,y,z}$, can be denoted as:

$$\mathbf{S}_{x,y} = \mathbf{I}_{x,y,(z)} \quad (17)$$

where the bracketed term specifies the index for the slice location. These slices are then decomposed along both dimensions and then combined to form a new 3D array $\mathbf{E}_{m,n,z}$, by performing [31]:

$$\mathbf{E}_{m,n,(z)} = \mathbf{t}_x \mathbf{S}_{x,y} \mathbf{t}_y^* \quad (18)$$

where * indicates the matrix transpose and \mathbf{t}_x and \mathbf{t}_y are orthogonal matrices with rows equal to the 1D Chebyshev polynomials:

$$\mathbf{t}_x = \begin{Bmatrix} \frac{t_0(x)}{\sqrt{\rho_0}} \\ \frac{t_1(x)}{\sqrt{\rho_1}} \\ \vdots \\ \frac{t_{M-1}(x)}{\sqrt{\rho_{M-1}}} \end{Bmatrix}, x = \{0, 1, 2, \dots, M-1\} \quad (19)$$

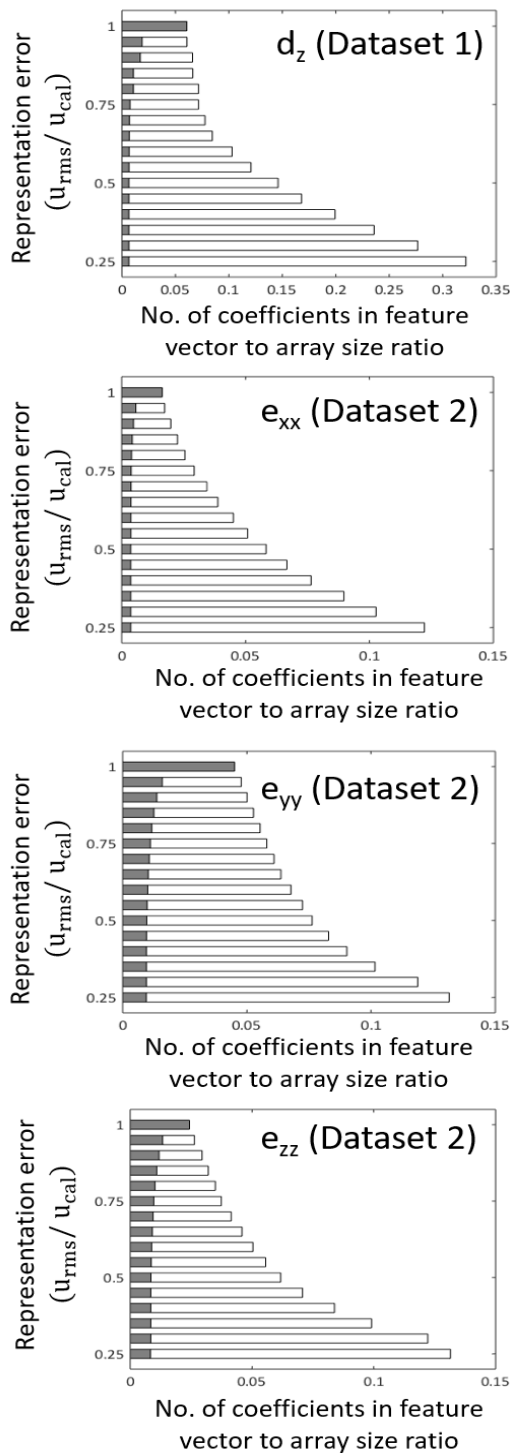


FIGURE 4. Bar charts showing the number of coefficients in the unprocessed feature vectors, defined as ratios of the data array size, with representation errors conforming to the CEN guide recommendation i.e. within the shaded segment of Fig. 3. The fill level in the bars, shaded in dark grey, indicates the proportion of significant coefficients retained in a feature vector after refinement. Dataset 1 is from the panel and Dataset 2 from the reinforced rubber matrix.

$$\mathbf{t}_y = \begin{Bmatrix} \frac{t_0(y)}{\sqrt{\rho_0}} \\ \frac{t_1(y)}{\sqrt{\rho_1}} \\ \vdots \\ \frac{t_{N-1}(y)}{\sqrt{\rho_{N-1}}} \end{Bmatrix}, y = \{0, 1, 2, \dots, N-1\} \quad (20)$$

The 3D array $\mathbf{E}_{m,n,z}$, is then decomposed in the z-direction by performing:

$$\mathbf{T}_{m,n,(o)} = \frac{1}{\sqrt{MNO}} (\mathbf{t}_z \mathbf{E}_{m,(n),z}^*)^* \quad (21)$$

where,

$$\mathbf{t}_z = \begin{Bmatrix} \frac{t_0(z)}{\sqrt{\rho_0}} \\ \frac{t_1(z)}{\sqrt{\rho_1}} \\ \vdots \\ \frac{t_{O-1}(z)}{\sqrt{\rho_{O-1}}} \end{Bmatrix}, z = \{0, 1, 2, \dots, O-1\} \quad (22)$$

3D array \mathbf{T} contains the same coefficients as obtained using equation (8) and can be permuted to a feature vector using the same conditions as described by equations (10) and (11). This results in a significant decrease in computation time. For example, when decomposing a cube of data of dimension 200 pixels into a feature vector containing 200 coefficients the matrix-based algorithm was found to be 150 times faster than using equation (8) and gave the same result. The number of rows in the matrices \mathbf{t}_x , \mathbf{t}_y and \mathbf{t}_z can be reduced to calculate a smaller number of coefficients. This is useful for orthogonal decomposition of experimental mechanics data, as typically only polynomials up to a maximum order of twenty are required for an accurate reconstruction due to the inherent properties of data fields constrained by continuum mechanics. The data volume can be reconstructed in a similar manner but in reverse:

$$\mathbf{E}_{m,(n),z} = \sqrt{MNO} \mathbf{T}_{m,(n),o} \mathbf{t}_z \quad (23)$$

with the reconstructed volume given by:

$$\hat{\mathbf{I}}_{x,y,(z)} = \mathbf{t}_x^* \mathbf{E}_{m,(n),z} \mathbf{t}_y^* \quad (24)$$

III. Exemplar volumetric datasets

Two types of volumetric datasets are briefly described here, which were used as exemplars to demonstrate the application of orthogonal decomposition in quantitative validation of computational mechanics models.

A. DATASET 1: MODAL ANALYSIS OF AN AEROSPACE PANEL

A schematic of the panel is shown in Fig. 1. The surface of the panel was sprayed with a random black and white speckle

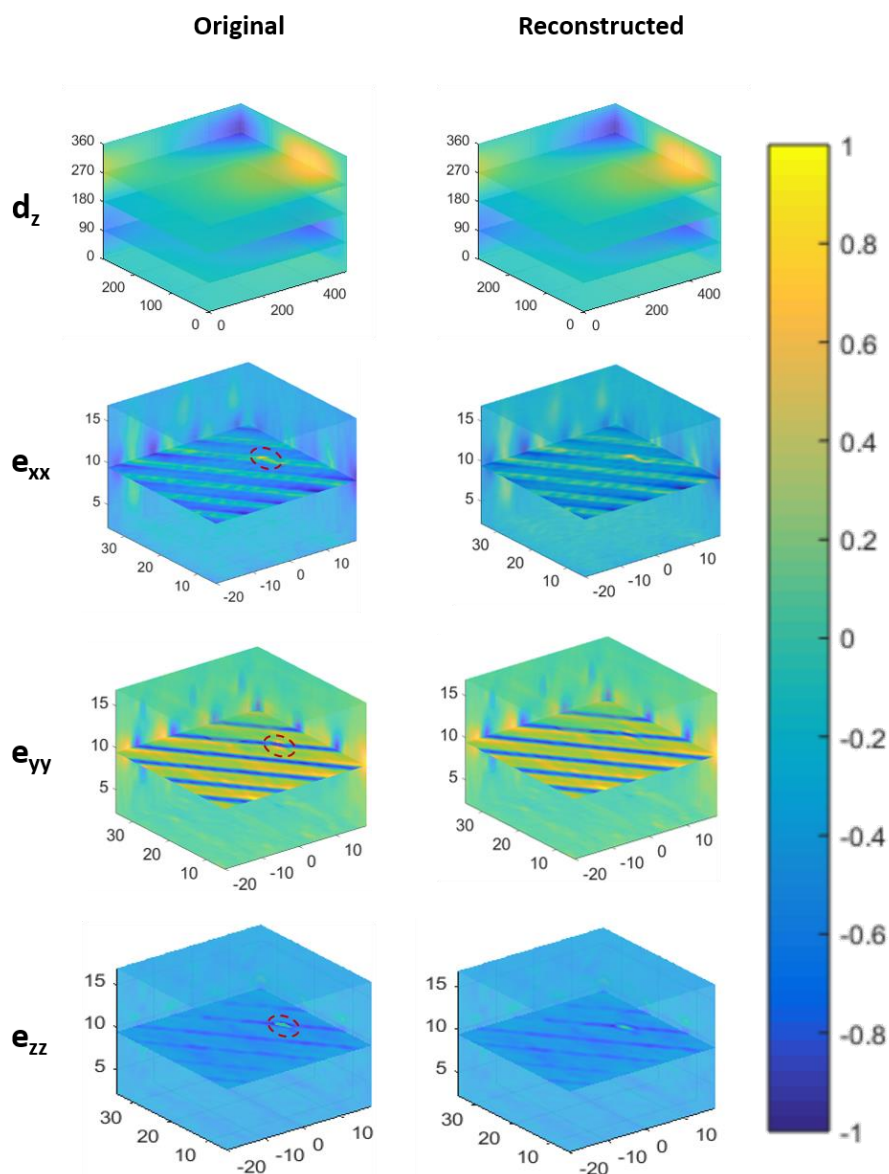


FIGURE 5. Measured (left) and reconstructed (right) data arrays from the refined featured vectors with $u_{rms} \approx u_{cal}$. The region encircled by the dashed-red line in the strain arrays highlights the presence of a highly localized feature in the strain distributions. This figure is best interpreted in colour. The displacement data (top) is from the panel and the strain data from the reinforced rubber matrix.

pattern and the panel was suspended using string from a rigid frame, which was affixed to an optical table. The panel was excited at its third resonant frequency of 59 Hz using an electromagnetic shaker (V100, DataPhysics, CA). During excitation, images of the painted surface were captured using a stereoscopic pulsed-laser DIC system [32], which was designed to acquire full-field periodic displacements of the panel by phase shifting the image acquisition with respect to the excitation signal. The optical setup comprised of two identical digital cameras (Stingray F-201B, AVT, Germany) with 1624×1234 pixel resolutions, mounted with an identical pair of 8 mm focal length lenses (Cinegon 1.4/8, Schneider, Germany). The two cameras were positioned at a working distance of about 1500 mm from the panel at a stereo angle of

25° , providing an image magnification of approximately of 3.1 pixels/mm. A 532 nm laser (Nano L-200-10, Litron, England) with a pulse duration of 4 ns was used to illuminate and consequently “freeze” the motion of the vibrating panel in order to acquire images of the panel’s surface. A total of 41 pairs of images were acquired with the commercial DIC software, Istra4D (Dantec Dynamics, Germany) using an incremental phase shift of 9° to cover a complete (360°) loading cycle of the panel. The image correlation was performed with Istra4D using a subset size of 49 pixels and a pitch of 20 pixels. The out-of-plane displacement maps from Istra4D were stacked in the z-direction at fixed intervals of 9° to construct a 3D array comprising of 1.18×10^5 data points, shown in Fig 1.

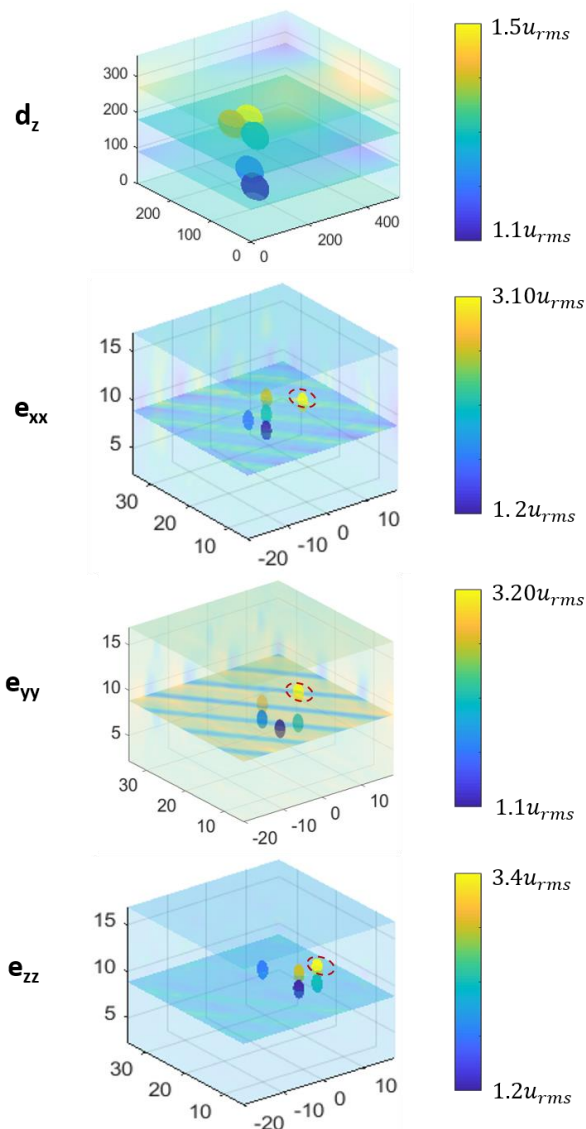


FIGURE 6. Plots showing the location of five clusters of adjacent data points, represented by spheres, comprising 0.3% of the total number of points in the array with the highest residual. The cluster residual is defined as a ratio of the average representation error, u_{rms} for the reconstructed arrays shown in Fig. 5. For the strain arrays, the location of the cluster with the highest residual error corresponds with the location of the highly localized feature in the strain distribution, encircled by the dashed-red line in Fig. 5. The displacement data (top) is from the panel and the strain data from the reinforced rubber matrix. This figure is best interpreted in colour.

A FE model was created using 170,000 first-order hexahedral elements using a commercial FE package (Altair, Optistruct, USA). An eigenvalue analysis was first performed to identify the resonant frequencies of the panel, followed by a modal frequency response analysis to acquire full-field out-of-plane displacements at its third resonant frequency of 59 Hz. Further information about the experimental setup and FE model can be found in the paper by Sebastian *et al.* [32]. The simulation data from the modal frequency response analysis was available in the form of 21 grey-scale images, representing the contour maps of the out-of-plane

displacement of the panel at uniform phase intervals of 18° . The images were imported into Matlab and were subsequently cropped after identifying a rectangular region, corresponding to the region of interest from which the measured displacement data was acquired, using the Matlab image registration function. A 3D array comprising of 7.96×10^6 data points was constructed from the predicted data by stacking rectangular segments from each of the 21 grey scale images in the z-direction at regular phase intervals of 18° . The constructed volumes for both the measured and predicted data are shown in Fig. 1. Normalization was performed on both datasets to transform them such that their values ranged between -1 and 1. This was to enable comparisons between the predicted and experimental data.

B. DATASET 2: REINFORCED-RUBBER MATRIX SPECIMEN UNDER TENSILE LOAD

A cuboid-shaped tensile test specimen was fabricated from silicone (RTV-664, Momentive, USA) with the dimensions of $139.7 \times 38.1 \times 19.6$ mm. The rubber matrix was reinforced using three layers of three-strand twist nylon cord with a nominal diameter of 2.3 mm. The cords in the bottom, middle and top layers were orientated at 90° , 45° and 90° from the longitudinal (y) axis of the specimen and were located at heights of 5.6, 9.9 and 13.3 mm from the bottom surface, respectively. During fabrication, glass micro-beads with a nominal diameter of 200 μm were added to the rubber mix. Upon curing, the combined distribution of matrix voids and glass beads provided a sufficiently high-contrast random pattern to perform DVC. The specimen was mounted in a custom-built loading frame, which was in turn mounted onto the rotation stage of an X-ray micro-computed tomography system (X-TEK HMX 160). CT scans were obtained prior to and after the application of a tensile load of 150 N along the longitudinal (y) direction. The cuboid scan region within the specimen was $4.7 \text{ mm} \leq x \leq 34.9 \text{ mm}$, $-20.5 \text{ mm} \leq y \leq 18.4 \text{ mm}$ and $1.96 \text{ mm} \leq z \leq 15.16 \text{ mm}$, this region is marked in the specimen schematic in Fig. 2. The acquired CT images with a voxel resolution of 57.7 μm were processed using a commercial DVC package, VIC-Volume (Correlated Solutions, USA). The displacements were computed using a cubic subset size of 13 voxels and a pitch of 7 voxels. Strains were evaluated using VIC-Volume by locally smoothing the displacements using a grid of $5 \times 5 \times 5$ data points. The evaluated displacement and strain data, exported from VIC-Volume, was in the form of 3D arrays with each array comprising of 7.78×10^5 data points.

A FE model of the rubber matrix specimen was developed using a custom modelling tool based on the Virtual Textile Morphology Suite (VTMS) and the B-spline Analysis Method (BSAM), which were developed by the Air Force Research Lab (AFRL). Further details about the specimen preparation, experimental setup and FE model can be found in the paper by Mollenhauer *et al.* [33]. The simulation data was made available by the AFRL in the form of a text file containing

Cartesian coordinates for all 4.94×10^5 nodes of the FE model along with the corresponding predicted displacement and strain values at those nodes. The data was imported into a Matlab algorithm which constructed 3D arrays from the simulation data. The comparison between normalized measured and FE predicted arrays of strain components along three orthogonal directions is shown in Fig 2.

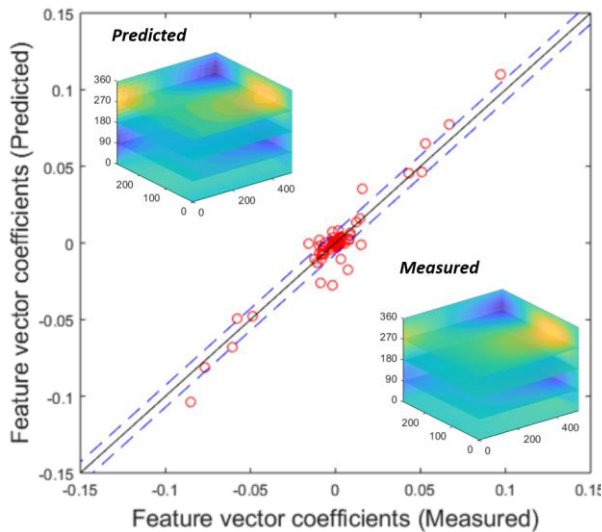


FIGURE 7. Graph of coefficients of the refined feature vectors representing the measured and predicted displacement arrays for the aerospace panel, shown in Fig. 1, plotted against one another. The dashed lines represent the total expanded uncertainty, $2u_{exp}$.

IV. DECOMPOSING VOLUMETRIC ARRAYS INTO FEATURE VECTORS

Two approaches to decomposing volumes of data using Chebyshev polynomials are introduced in Sect. II. Whilst both approaches yield the same coefficients when applied to a dataset, they differ substantially in terms of the computing time required. When decomposing the data for the reinforced rubber matrix on a PC with an Intel® Core™ i5-8400 CPU and 8GB of RAM, the approach based on equation (8) took 1004s whereas the matrix-based approach using equations (17) to (21) took less than 0.1s. This disparity stems from two factors. Firstly, equation (8) requires each kernel to be calculated separately for each coefficient, whereas the matrix-based approach does not. The second factor is that the matrix-based approach ensures that the large numbers of multiplications and additions necessary for decomposition can be performed using the computationally efficient vector processing instructions built into modern computer processors.

When an array of acquired data, for example experimental measurements or simulation predictions, is orthogonally decomposed into a feature vector, it is important to determine whether the feature vector provides an acceptable representation of the original data. The CEN CWA-16799 workshop agreement [29], which is essentially a guide for the

validation of computational mechanics models, recommends two criteria to ensure that a feature vector accurately represents both the global and local features in an original data array. The first criterion states that a feature vector is considered to be an acceptable representation of the measured data array if the representation error, u_{rms} does not exceed the minimum measurement uncertainty, u_{cal} of the measurement system. The representation error can be evaluated by calculating the root-mean-square of the difference between the original and the reconstructed array from equation (14) or directly using the feature vector from equation (16). According to second criterion, there should be no clusters of data points in the reconstructed array where the difference or the residual is greater than three times the representation error. A cluster is defined in the CEN guide as a region of adjacent data points representing at least 0.3% of the total number of points in the array. To perform orthogonal decomposition based on the CEN guide recommendations, it was essential to first establish u_{cal} for the measured data arrays. For Dataset 1, u_{cal} had been previously evaluated to be $4 \mu\text{m}$ or 1% of the measured data range based on the DIC calibration procedure proposed by Sebastian and Patterson [34]. A reliable estimate of u_{cal} was not available for the arrays measured using digital volume correlation in Dataset 2; therefore, it was assumed to be 1% of the median of the data ranges for the three measured strain arrays. The plots in Fig. 3 show the consistent trend of decreasing representation error with an increase in the number of coefficients in the feature vector for the four measured data arrays in Datasets 1 and 2. In these plots, the number of coefficients in a feature vector has been presented as a ratio of the measured data array size and the representation error, u_{rms} has been stated as a ratio of the minimum measurement uncertainty, u_{cal} . The shaded region in Fig. 3 represents the segment of the plots with feature vectors conforming to the requirement in the CEN guide for u_{rms} to not exceed u_{cal} . For 2D data fields, it has been a common practice [35] to perform decomposition using a large number of kernels such that u_{rms} is significantly lower than u_{cal} . A threshold level is then defined to set those coefficients in the feature vector to zero whose absolute magnitude is lower than the threshold. This results in a relatively small number of significant coefficients in the refined feature vector. In this approach, the threshold value needs to be identified such that u_{rms} of the reconstruction from the refined feature vector is equal to the measurement uncertainty (u_{cal}) to confirm with the CEN guide recommendation. This is done by choosing an initial value of the threshold to determine the resulting u_{rms} of the reconstruction from the refined feature vector, which is then adjusted in an iterative manner to make u_{rms} equal to u_{cal} .

An alternate approach, to identifying the smallest set of significant coefficients from an unprocessed feature vector, is used in this work which ensures that u_{rms} of the refined feature vector remains less than u_{cal} . In this approach,

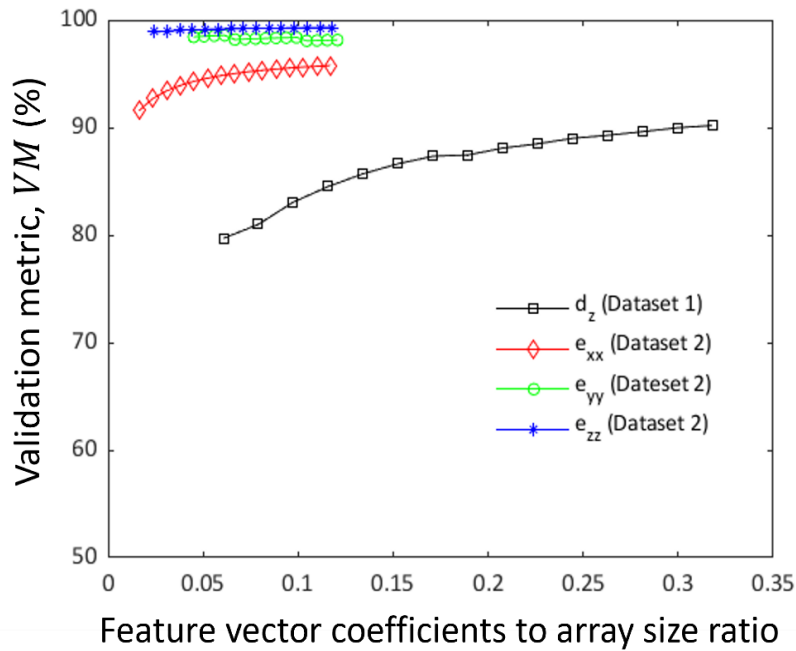


FIGURE 8. Plot showing the values of validation metric at feature vector length to data array size ratios within the shaded segment of Fig. 3 for the four pairs of measured and predicted data arrays shown in Figures 1 and 2. Dataset 1 is from the panel and Dataset 2 from the reinforced rubber matrix.

coefficients are selected one by one from the original (unprocessed) feature vector based on their absolute magnitudes, such that the coefficients with the highest absolute magnitude are selected first. After each selection, u_{rms} is evaluated using equation (16) and compared with u_{cal} . The selection process is stopped when u_{rms} becomes less than u_{cal} .

The feature vectors for the four measured data arrays, with u_{rms} less than or almost equal to u_{cal} , i.e., the ones belonging to the shaded region in Fig. 3, were processed using the proposed feature vector refinement approach. The shaded segment of the plots in Fig. 3 are replotted as bar charts in Fig. 4 in which the height of the bar represents the number of coefficients in the unprocessed feature vector, defined as the ratio of the data array size. The fill level in the bars, highlighted in dark grey, represents the proportion of coefficients retained in a feature vector after the refinement process. It can be observed from the fill levels in these bar charts that retained coefficients converged to a constant number of significant coefficients. It is difficult to establish this convergence with the threshold-based approach [35] primarily because the threshold level at which $u_{rms} \approx u_{cal}$ is a function of the number of coefficients in the unprocessed feature vector. The size of the converged set of most significant coefficients for the four measured datasets are reported in Table 2. The ratios of the size of these converged sets of coefficients to the original array size are also provided in Table 2, which provide a measure of the reduction in dimensionality offered by this volumetric decomposition

process. The arrays reconstructed from the refined feature vectors are compared with the original arrays in Fig. 5.

To inspect the cluster residuals in the reconstructed data arrays shown in Fig. 5, a spherical element was first defined such that the number of adjacent points lying within this spherical element are 0.3% of the total number of points in the array. The spherical element was moved to every location in the array grid and the cluster residual was evaluated by taking the root-mean-square of the difference between the original and the reconstructed array using the data points lying within the spherical element. Fig. 6 shows the locations of the five clusters with the highest residuals for the four reconstructed data arrays presented in Fig. 5. For the arrays of strain components, a single cluster of adjacent data points was identified where the residual slightly exceeded the CEN recommended maximum limit of $3u_{cal}$. This cluster was found to be located where a highly localized feature in the strain distributions was present, which is encircled by the dashed-red line in Fig. 5 and 6. As described in Sect II, the proposed decomposition algorithm is based on the discrete Chebyshev polynomials, which is more suited to representing the global features in the dataset. If there is a significant number of highly localized features with sharp edges in a dataset, such as the ones highlighted in Fig. 5, then there are other discrete polynomials in the literature e.g. Krawtchouk moments [27], which are more suited to defining such localized features.

V. COMPARISON OF MEASURED AND PREDICTED VOLUMETRIC DATA

The applicability of methodologies [19], [29], which were developed for quantitative comparison of 2D data fields utilizing orthogonal decomposition, are analyzed in this section for the volume data arrays. The CEN CWA-16799 guide [29] has outlined a method for making a comparison between the measured and predicted 2D data fields for the purpose of validation of computational solid mechanics models. In this method, the measured and predicted data fields are first represented as feature vectors by performing orthogonal decomposition. The coefficients of the two feature vectors are then plotted against one another for a simple graphical comparison. The CEN guide recommends that the computational model is considered acceptable if all of the pairs of coefficients in the two feature vectors fall within the uncertainty zone defined by:

$$f_{P_i} = f_{S_i} \pm 2u_{exp}, i = 1, 2, \dots, l \quad (25)$$

where f_{P_i} and f_{S_i} are the i th coefficients in the feature vectors representing the predicted and the measured data fields, respectively, and l is the total number of coefficients in the feature vector. u_{exp} is the total uncertainty which can be determined by:

$$u_{exp} = \sqrt{u_{cal}^2 + u_{rms}^2} \quad (26)$$

where u_{cal} is the minimum uncertainty in the measured data field and u_{rms} is the representation error in the reconstructed data field.

To illustrate this method for volumetric datasets, the coefficients of the feature vectors representing the measured and FE predicted displacement arrays in Dataset 1 are plotted against one another in Fig. 7. It can be observed from the plot in Fig. 7 that some of the points are outside the uncertainty zone, defined by the two dashed lines, which, according to the CEN guide criterion, makes the predictions of the FE model unacceptable. This approach does not provide any information about the degree to which the prediction results represent the measured data or in this case, how bad is the FE model. To fill this gap, a probabilistic validation approach [19] has been developed which evaluates a validation metric, VM representing the probability that the prediction results belong to the same population as the measured data. Four steps are involved in determining VM , which are briefly described here. In the first step, the normalized relative error, e_i for each pair of coefficients in the feature vectors representing the measured and predicted data are calculated using:

$$e_i = \left| \frac{f_{P_i} - f_{S_i}}{\max_j |f_{S_j}|} \right| \quad (27)$$

The weight, w_i for each of the normalised error terms are then determined using:

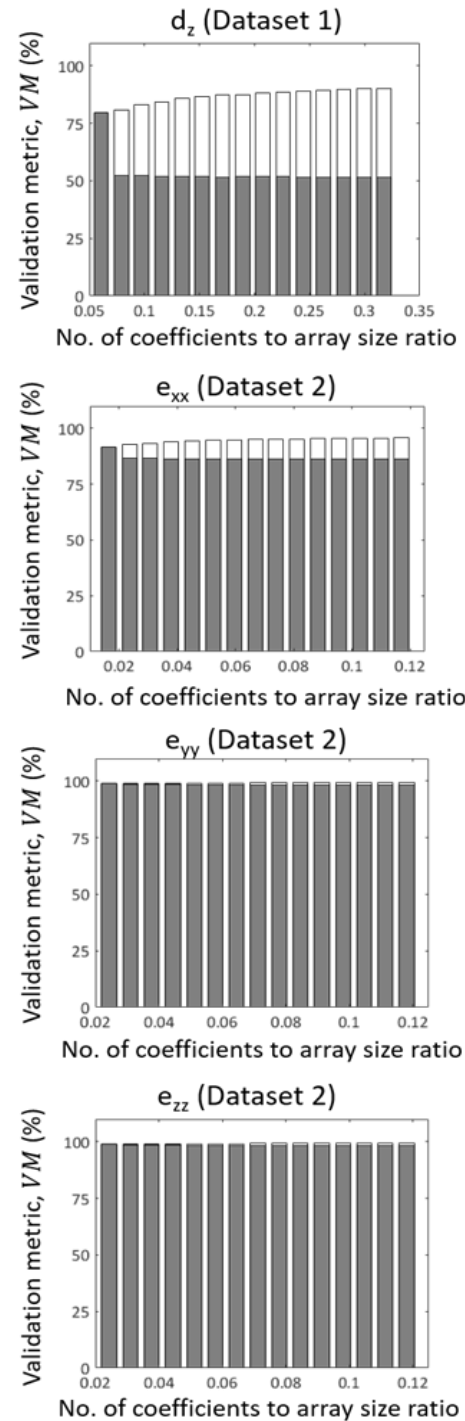


FIGURE 9. Bar charts showing the validation metric, VM determined from unprocessed feature vector pairs, representing the measured and predicted data arrays, at feature vector length to array size ratios within the shaded segment of Fig. 3. The fill level in the bars, shaded in dark grey, indicates the values of VM determined after removing the insignificant coefficients from the feature vector pairs by employing the refinement approach described in the fourth section. Dataset 1 is from the panel and Dataset 2 from the reinforced rubber matrix.

$$w_i = \frac{e_i}{\sum_{i=1}^n e_i} \times 100 \quad (28)$$

In the third step, an error threshold, e_{thresh} is defined by dividing the expanded total uncertainty, $2u_{exp}$ by the coefficient in the feature vector for the measured data with the maximum absolute magnitude,

$$e_{thresh} = \frac{2u_{exp}}{\max_i |f_{s_j}|} \quad (29)$$

In the last step, VM is determined by summing the weights for all of the normalized errors terms that are found to be below the defined error threshold:

$$VM = \sum_i (w_i \parallel e_i < e_{thresh}) \quad (30)$$

where \parallel is an indicator function which takes the value 1 when $e_i < e_{thresh}$ and otherwise has a value zero.

From experience with historical 2D data, acquired from full-field techniques such as DIC and TSA, it has been established that 2D displacement and strain fields can be decomposed into feature vectors with low representation errors using, typically, less than a hundred Chebyshev polynomials-based kernels. The feature vectors representing volumetric data arrays can have more than a thousand coefficients (see Table 2), which is consistent with the increased number of grid points in a volume with addition of the third dimension. In order to correctly apply the above-described probabilistic validation approach to volumetric arrays, it is important to first analyze the sensitivity of VM to the number of coefficients in the feature vector pair of measured and predicted data.

The four predicted data arrays shown in Fig. 1 and 2 were decomposed into feature vectors with the same of number of kernels as the ones for the measured data arrays plotted within the shaded segment of Fig. 3. VM was then evaluated for each corresponding feature vector pair representing the pair of measured and predicted data arrays. The plot in Fig. 8 shows the sensitivity of VM to the total number of coefficients in the feature vectors representing the measured and predicted data. The number of normalized error terms (e_i) that are found to be below the error threshold (e_{thresh}) increases with the inclusion of more coefficients in the unprocessed feature vector. This causes the accumulative weight of the error terms below the error threshold to increase as well, which is defined as the validation metric, VM according to equation (30). Hence, in order to acquire unbiased values for VM , it is imperative to exclude those coefficients in the feature vector pairs representing the measured and predicted arrays, whose associated kernels do not make a significant contribution in defining the inherent distribution in the original arrays.

TABLE 3.
Validation metric for the four predicted data arrays in exemplar datasets.

Exemplar	Data	VM (%)
Panel	Out-of-plane displacement (d_z)	51.7
	Strain along x-direction (e_{xx})	86.3
Reinforced rubber matrix	Strain along y-direction (e_{yy})	97.6
	Strain along z-direction (e_{zz})	98.4

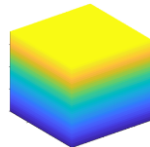
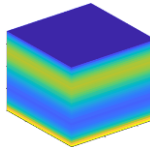
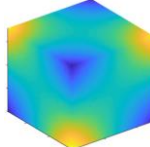
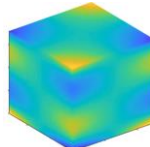
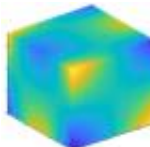
It was established in the previous section that with the proposed approach for feature vector refinement, a smallest set of significant coefficients can be identified for an arbitrary representation error. With this set of significant coefficients, an unbiased, converged value for VM can be obtained. The values for VM obtained using the unprocessed pair of feature vectors are replotted in Fig. 9 as bars. The fill level of the bars, highlighted in dark grey colour, represents the values for VM which were determined after excluding the insignificant coefficients from the feature vectors. It can be observed from the fill levels in bar charts of Fig. 4 and 9 that VM converges to a constant value as the retained coefficients in the refined feature vector converge to a constant set of significant coefficients. The converged values of VM are not dependent on the feature vector length and hence provide an unbiased quantitative measure of the confidence associated with the agreement between the predicted and measured results. The converged values of VM for the four predicted data arrays in Datasets 1 and 2 are provided in Table 3.

VI. DISCUSSION

The quantitative comparison of large datasets has been a challenging task for researchers primarily because datasets from different sources often do not share the same grid size, data pitch or coordinate system. A rudimentary approach for data comparison, which is still predominant in industry and academia, involves identifying critical locations in the measured datasets and qualitatively establishing the agreement between the predicted and measured data points at these critical locations. This paper reports the development of an algorithm which decomposes a volumetric array into a set of coefficients by fitting a predefined set of 3D kernels, which are formed from 1D discrete Chebyshev polynomials. The set of coefficients are collated into a column vector, referred to as the feature vector, based on the ordering system defined by Bateman [29], which has been extended to three dimensions in this work. Since this arrangement of coefficients in a feature vector is fixed, this allows one-to-one comparison of the volumetric arrays within the feature vector space, irrespective of whether they share the same grid size, data pitch or coordinate system.

TABLE 4

Visualization of the discrete Chebyshev-based 3D kernels belonging to the five most dominant coefficients in the refined feature vector representing the out-of-plane displacement array, d_z in the aerospace panel. The absolute magnitudes of the coefficients listed in the table are normalized by the coefficient in the feature vector with the maximum absolute magnitude. This table is best interpreted in colour.


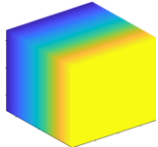
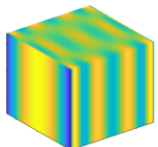
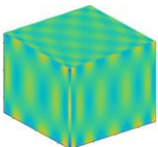
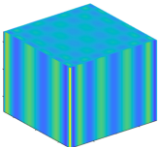
Normalized absolute magnitude of coefficients	Order of corresponding kernel $\omega_{m,n,o}$	Shape of the corresponding kernel
1	$\omega_{0,0,1} = 1$	
0.880	$\omega_{0,0,3} = 3$	
0.790	$\omega_{1,1,1} = 3$	
0.690	$\omega_{1,1,3} = 5$	
0.626	$\omega_{2,1,3} = 4$	

The number of coefficients required in a feature vector to accurately represent the original data array depends on the ‘shape’ of the distribution in an array. In general, the distribution in a strain array, being derived from partial derivatives of displacements, tends to have a higher spatial variation compared to that in a displacement array. Hence, strain arrays are typically represented using a set of coefficients associated with relatively high order kernels. To illustrate this with an example, the order of the kernels associated with the five most significant coefficients in the refined feature vector representing the displacement array (d_z) and the strain array (e_{yy}) are shown in Tables 4 and 5, respectively. The order of the kernel for the fifth most significant kernel was found to be 4 and 17 for the out-of-plane displacement (d_z) and the in-plane strain (e_{yy}), respectively. The arrays in the second dataset, shown in Fig. 2, contain localized strains around the nylon cord reinforcements. In order to accurately represent these strain localizations, the

strain arrays in Dataset 2 required up to nine times as many kernels as required by the displacement array in Dataset 1.

The plots in Fig. 3 show that the representation error (u_{rms}) decreases in an exponential manner with the increase in the number of kernels used for decomposition. It can be observed in Fig. 3 that these plots, particularly for d_z , exhibit a jagged profile. This jaggedness is caused by the inclusion of coefficients whose associated kernel makes a significant contribution to representing the inherent distribution in the original data array, thereby causing a significant drop in u_{rms} when those coefficients are included. The refinement approach described in the section IV identifies the smallest set of significant coefficients that results in an arbitrary u_{rms} , maximizing the reduction in the dimensionality of the data within the feature vector space. In this study, refinement of the unprocessed feature vector was performed so that u_{rms} was just less than the minimum measurement uncertainty (u_{cal}) of the measurement system, as per the recommendations of the CEN CWA-16799 guide [29], which states that u_{rms} should

TABLE 5
Visualization of the discrete Chebyshev-based 3D kernels belonging to the five most dominant coefficients in the refined feature vector representing the out-of-plane displacement array, d_z in the aerospace panel the strain array, e_{yy} in the reinforced rubber matrix. The absolute magnitudes of the coefficients listed in the table are normalized by the coefficient in the feature vector with the maximum absolute magnitude. This table is best interpreted in colour.

Normalized absolute magnitude of coefficients	Order of corresponding kernel $\omega_{m,n,o}$	Shape of the corresponding kernel
1	$\omega_{0,0,0} = 0$	
0.880	$\omega_{1,0,0} = 1$	
0.790	$\omega_{2,8,0} = 10$	
0.690	$\omega_{7,10,2} = 19$	
0.626	$\omega_{7,10,0} = 17$	

not exceed u_{cal} . The reduction in the number of coefficients in the refined feature vector, after removal of the redundant coefficients, has been illustrated using the bar charts in Fig. 4.

As mentioned earlier, one of the primary applications of the decomposition method lies in making meaningful comparisons of datasets. This has led to a recently-developed approach for quantitative validation of computational solid mechanics models [19]. In this approach, the measured and predicted data arrays are first represented by a pair of feature vectors obtained using orthogonal decomposition. The cumulative weight of the normalized differences between the individual coefficients of the two feature vectors, which are found to be below an error threshold based on the total measurement uncertainty, is then computed to obtain a validation metric, VM . The magnitude of VM represents the probability that the predicted data belong to the same population as the measured data; and hence, provide a quantitative measure of the quality of the predicted data. In this study, the applicability of this validation approach to volumetric data arrays was assessed. The validation metric,

VM was found to be sensitive to the number of coefficients in the unprocessed feature vector, which can be seen in the plot in Fig. 8. It was demonstrated in Fig. 9 that a stable and unbiased value of the validation metric, VM can be acquired by using the set of most significant coefficients in a feature vector.

The proposed orthogonal decomposition algorithm was developed with the aim of decomposing volumetric datasets which contain spatial variation in all three dimensions. Such datasets are typically produced by techniques such as automated serial-sectioning and X-ray computed tomography. However, the algorithm is equally applicable to 2D data fields which vary in the temporal domain and, for the purpose of orthogonal decomposition, can be treated as a volumetric array. In Dataset 1, a series of 41 2D out-of-plane surface displacement fields, acquired using DIC, of an aerospace panel excited at its third resonant frequency, were stacked in the z-direction to construct a volumetric data array shown in Fig. 1. The constructed array was orthogonally decomposed into a feature vector with 758 significant coefficients giving

representation error (u_{rms}) of the reconstructed array equivalent to the minimum measurement (u_{cal}) of the DIC system. The potential advantage of employing 3D orthogonal decomposition over its 2D counterpart was explored by individually decomposing each of the 41 slices in the x - y plane of the data array in Fig. 1 into feature vectors, with $u_{rms} \approx 0.25u_{cal}$, using the image decomposition algorithm based on the same 1D discrete Chebyshev polynomials which were used in the development of the volume decomposition algorithm. The unprocessed feature vectors for each slice were refined using the method reported in the section IV to achieve $u_{rms} \approx u_{cal}$. Each of the 41 refined feature vectors, representing the individual slices of the volume, contained on average 100 coefficients. Hence, the whole data array was represented by a total of 4100 coefficients in 41 feature vectors, which are five times more than the coefficients in a single feature vector resulting from volume decomposition. The 3D kernels in volume decomposition can represent distributions along all three dimensions of data array. This is primarily the reason why volume decomposition required a relatively small set of kernels to represent the data array compared to its 2D counterpart.

The volume decomposition algorithm offers great potential for increasing efficiency in analyzing large volumes of experimental data, such as that produced by experiments conducted on the dynamic response of components. High-speed cameras, which are capable of acquiring tens of thousands of images in a matter of seconds, are typically employed in such experiments. A set of deformation fields from images acquired over an arbitrary time interval can be constructed into volumetric segments, which can then be decomposed into feature vectors using orthogonal decomposition. This would not only allow significant data reduction but also reduce the time and effort required to interpret experimental data.

VII. CONCLUSIONS

This paper reports the development of an orthogonal decomposition algorithm based on discrete Chebyshev polynomials which can decompose volumetric data arrays into feature vectors. This allows for straightforward quantitative comparison of information-rich three-dimensional (3D) datasets within feature vector space, irrespective of whether they share the same grid size, data pitch or coordinate system. The quantitative data comparison capability of the decomposition algorithm was demonstrated using two pairs of exemplar measured and finite element (FE) predicted datasets. The experimental data in first pair of datasets comprised of time-varying out-of-plane surface displacement fields of a panel subjected to excitation at one of its resonant frequencies, which were acquired using digital image correlation. The experimental data in the second pair of datasets represented the internal 3D strain fields in a nylon cord reinforced-rubber matrix specimen subjected to a tensile load, which were measured using digital volume correlation technique. The

decomposition algorithm was successfully employed to perform quantitative validation of FE predicted data using a validation metric, which was previously developed for two-dimensional data fields. Future work will focus on the use of volume decomposition on X-ray micro-computed tomography data for characterizing damage in composite microstructures.

ACKNOWLEDGMENT

The authors are grateful to Dr Chris M Sebastian for providing the experimental and finite element data for the modal analysis of the aerospace panel.

REFERENCES

- [1] Z. Liu, D. S. Forsyth, J. P. Komorowski, K. Hanasaki, and T. Kirubarajan, "Survey: State of the Art in NDE Data Fusion Techniques," *IEEE Transactions on Instrumentation and Measurement*, vol. 56, no. 6, pp. 2435–2451, Dec. 2007, doi: 10.1109/tim.2007.908139.
- [2] W. Wang, J. E. Mottershead, A. Ihle, T. Siebert, and H. Reinhard Schubach, "Finite element model updating from full-field vibration measurement using digital image correlation," *Journal of Sound and Vibration*, vol. 330, no. 8, pp. 1599–1620, Apr. 2011, doi: 10.1016/j.jsv.2010.10.036.
- [3] A. Germaineau, F. Peyruseigt, S. Mistou, P. Doumalin, and J.-C. Dupre', "3D mechanical analysis of aeronautical plain bearings: Validation of a finite element model from measurement of displacement fields by digital volume correlation and optical scanning tomography," *Optics and Lasers in Engineering*, vol. 48, no. 6, pp. 676–683, Feb. 2010, doi:10.1016/j.optlaseng.2010.01.010.
- [4] K. A. Kasvayee, K. Salomonsson, E. Ghassemali, and A. E. W. Jarfors, "Microstructural strain distribution in ductile iron; comparison between finite element simulation and digital image correlation measurements," *Materials Science and Engineering A*, vol. 655, pp. 27–35, 2016, doi: 10.1016/j.msea.2015.12.056.
- [5] R. Zael, Y. N. Yeni, B. K. Bay, X. N. Dong, and D. P. Fyhrie, "Comparison of the Linear Finite Element Prediction of Deformation and Strain of Human Cancellous Bone to 3D Digital Volume Correlation Measurements," *Journal of Biomechanical Engineering*, vol. 128, no. 1, pp. 1–6, Jul. 2005, doi: https://doi.org/10.1115/1.2146001.
- [6] S. Oliviero, M. Giorgi, and E. Dall'Ara, "Validation of finite element models of the mouse tibia using digital volume correlation," *Journal of the Mechanical Behavior of Biomedical Materials*, vol. 86, pp. 172–184, Oct. 2018, doi: https://doi.org/10.1016/j.jmbbm.2018.06.022.
- [7] A. K. Jain, P. W. Duin, and Jianchang Mao, "Statistical pattern recognition: a review," *IEEE Transactions on Pattern Analysis and Machine Intelligence*, vol. 22, no. 1, pp. 4–37, 2000, doi: 10.1109/34.824819.
- [8] K. Taira et al., "Modal Analysis of Fluid Flows: An Overview," *AIAA Journal*, vol. 55, no. 12, pp. 4013–4041, Dec. 2017, doi: 10.2514/1.j056060.
- [9] I. T. Jolliffe and J. Cadima, "Principal component analysis: a review and recent developments," *Philosophical Transactions of the Royal Society A: Mathematical, Physical and Engineering Sciences*, vol. 374, no. 2065, p. 20150202, Apr. 2016, doi: 10.1098/rsta.2015.0202.
- [10] H. Chen, D. L. Reuss, and V. Sick, "On the use and interpretation of proper orthogonal decomposition of in-cylinder engine flows," *Measurement Science and Technology*, vol. 23, no. 8, p. 085302, May 2012, doi: 10.1088/0957-0233/23/8/085302.
- [11] G. Ceglia, S. Discetti, A. Ianiro, D. Michaelis, T. Astarita, and G. Cardone, "Three-dimensional organization of the flow structure in a non-reactive model aero engine lean burn injection system," *Experimental Thermal and Fluid Science*, vol. 52, pp. 164–173, Jan. 2014, doi: 10.1016/j.expthermflusci.2013.09.007.
- [12] G. Kerschen, J. Golinval, A. F. VAKAKIS, and L. A. BERGMAN, "The Method of Proper Orthogonal Decomposition for Dynamical Characterization and Order Reduction of Mechanical Systems: An

- Overview,” *Nonlinear Dynamics*, vol. 41, no. 1–3, pp. 147–169, Aug. 2005, doi: 10.1007/s11071-005-2803-2.
- [13] R. Allemang, M. M. Kolluri, M. Spottswood, and T. Eason, “Decomposition-based calibration/validation metrics for use with full-field measurement situations,” *The Journal of Strain Analysis for Engineering Design*, vol. 51, no. 1, pp. 14–31, Sep. 2015, doi: 10.1177/0309324715595141.
- [14] C. Schwarz, P. Ackert, and R. Mauermann. “Principal component analysis and singular value decomposition used for a numerical sensitivity analysis of a complex drawn part,” *The International Journal of Advanced Manufacturing Technology*. Vol. 94, no. 5, pp. 2255–2265, 2018, doi: 10.1007/s00170-017-0980-z.
- [15] R. Mukundan, S. H. Ong, and P. A. Lee, “Image analysis by Tchebichef moments,” *IEEE Transactions on Image Processing*, vol. 10, no. 9, pp. 1357–1364, Sep. 2001, doi: 10.1109/83.941859.
- [16] W. Wang, J. E. Mottershead, C. M. Sebastian, and E. A. Patterson, “Shape features and finite element model updating from full-field strain data,” *International Journal of Solids and Structures*, vol. 48, no. 11–12, pp. 1644–1657, 2011, doi: 10.1016/j.ijsolstr.2011.02.010.
- [17] P-T. Yap, R. Paramesran, and S.-H. Ong, “Image Analysis Using Hahn Moments,” *IEEE Transactions on Pattern Analysis and Machine Intelligence*, vol. 29, no. 11, pp. 2057–2062, Nov. 2007, doi: 10.1109/tpami.2007.70709.
- [18] C. Sebastian, E. Hack, and E. Patterson, “An approach to the validation of computational solid mechanics models for strain analysis,” *The Journal of Strain Analysis for Engineering Design*, vol. 48, no. 1, pp. 36–47, Jul. 2012, doi: 10.1177/0309324712453409.
- [19] K. Dvurecenska, S. Graham, E. Patelli, and E. A. Patterson, “A probabilistic metric for the validation of computational models,” *Royal Society Open Science*, vol. 5, no. 11, p. 180687, Nov. 2018, doi: 10.1098/rsos.180687.
- [20] K. Amjad, P. Lambert, C. A. Middleton, R. J. Greene, and E. A. Patterson, “A thermal-emissions based real-time monitoring system for in-situ detection of fatigue cracks,” *Proceedings of the Royal Society A*, vol. 478, no. 2266, 2022, doi: 10.1098/rspa.2021.0796.
- [21] W. J. R. Christian, K. Dvurecenska, K. Amjad, J. Pierce, C. Przybyla, and E. A. Patterson, “Real-time quantification of damage in structural materials during mechanical testing,” *Royal Society Open Science*, vol. 7, no. 3, p. 191407, Mar. 2020, doi: 10.1098/rsos.191407.
- [22] P. Lava, E. M. C. Jones, L. Wittevrongel, and F. Pierron, “Validation of finite-element models using full-field experimental data: Levelling finite-element analysis data through a digital image correlation engine,” *Strain*, vol. 56, no. 4, Apr. 2020, doi: 10.1111/str.12350.
- [23] M. Salloum, K.N. Karlson, H. Jun, J.A. Brown, D.S. Bolintineanu, and K.N. Long, “Comparing field data using Alpert multi-wavelets,” *Computational Mechanics*, vol. 66, pp. 893–910, 2020, doi: 10.1007/s00466-020-01878-2
- [24] B. J. Inkson, M. Mulvihill, and G. Möbus, “3D determination of grain shape in a FeAl-based nanocomposite by 3D FIB tomography,” *Scripta Materialia*, vol. 45, no. 7, pp. 753–758, Oct. 2001, doi: 10.1016/s1359-6462(01)01090-9.
- [25] I. R. Donis-González, D. E. Guyer, A. Pease, and F. Barthel, “Internal characterisation of fresh agricultural products using traditional and ultrafast electron beam X-ray computed tomography imaging,” *Biosystems Engineering*, vol. 117, pp. 104–113, Jan. 2014, doi: 10.1016/j.biosystemseng.2013.07.002.
- [26] J. E. Spowart, “Automated serial sectioning for 3-D analysis of microstructures,” *Scripta Materialia*, vol. 55, no. 1, pp. 5–10, Jul. 2006, doi: 10.1016/j.scriptamat.2006.01.019.
- [27] M. Flores, D. Mollenhauer, V. Runatunga, T. Bebermiss, D. Rapking, and M. Pankow, “High-speed 3D digital image correlation of low-velocity impacts on composite plates,” *Composites Part B: Engineering*, vol. 131, pp. 153–164, Dec. 2017, doi: 10.1016/j.compositesb.2017.07.078.
- [28] E. A. Moysenchik, V. P. Vavilov, and M. V. Kuimova, “Infrared Thermographic Testing of Steel Structures by Using the Phenomenon of Heat Release Caused by Deformation,” *Journal of Nondestructive Evaluation*, vol. 37, no. 2, Apr. 2018, doi: 10.1007/s10921-018-0482-4.
- [29] *Validation of computational solid mechanics models - CEN-CWA-16799*, Comité Européen de Normalisation, 2014.
- [30] H. Bateman, Erdélyi A., and Bateman Manuscript Project, *Higher transcendental functions*. Mineola, N.Y.: Dover Publications, 2006.
- [31] P-T Yap, R. Paramesran, and Seng-Huat Ong, “Image analysis by krawtchouk moments,” *IEEE Transactions on Image Processing*, vol. 12, no. 11, pp. 1367–1377, Nov. 2003, doi: 10.1109/tip.2003.818019.
- [32] C. M. Sebastian, E. López-Alba, and E. A. Patterson, “A comparison methodology for measured and predicted displacement fields in modal analysis,” *Journal of Sound and Vibration*, vol. 400, pp. 354–368, Jul. 2017, doi: 10.1016/j.jsv.2017.03.024.
- [33] D. Mollenhauer, D. Safriet, M. Sutton, H. Schreier, M. Kistner, and E. Zhou, “Characterization of strain distribution in a reinforced rubber-matrix composite using digital volume correlation,” in *Proceedings of the 29th Annual American Society of Composites Conference*, 2014.
- [34] C. M. Sebastian and E. A. Patterson, “Calibration of a Digital Image Correlation System,” *Experimental Techniques*, vol. 39, no. 1, pp. 21–29, Dec. 2012, doi: 10.1111/ext.12005.
- [35] W. J. R. Christian, F. A. DiazDelaO, and E. A. Patterson, “Strain-based damage assessment for accurate residual strength prediction of impacted composite laminates,” *Composite Structures*, vol. 184, pp. 1215–1223, Jan. 2018, doi: 10.1016/j.compstruct.2017.10.022.



Khurram Amjad received a MEng in Mechanical Engineering from the University of Sheffield in 2012 and a PhD specializing in experimental solid mechanics from the University of Liverpool in 2018. He has worked as a research associate at the University of Liverpool from 2018–2022 and is currently working as a Materials Engineer at the UK Atomic Energy Authority. His research interests include experimental solid mechanics, non-destructive evaluation and mechanical testing of fusion-relevant materials.



William J. R. Christian received a MEng in mechanical engineering from the University of Liverpool in 2014. He subsequently embarked on a PhD developing inspection techniques for aerospace materials, graduating from the University of Liverpool in 2017. After briefly working as a research associate, he became a lecturer at the University of Liverpool in 2018. His research interests are in the application of experimental solid mechanics, non-destructive evaluation, and composite materials to aerospace engineering problems.



Ksenija Dvurecenska received the MEng degree in aerospace engineering from the University of Southampton, UK, in 2013 and the Ph.D. degree in validation of solid mechanics models from the University of Liverpool, UK, in 2019. She has been a Lecturer at the University of Liverpool since 2016, and her research interests include quantitative validation methodologies, effective use of the measured data in the validation process and interpretation of the validation outcomes to support decisions based on the predictions of the computational models. Dr. Dvurecenska was a recipient of the National Nuclear Laboratory Chief Scientist Award for the best paper in 2018 resulting from an NNL-university collaboration.



David H. Mollenhauer grew up in central Texas and received a B.S. degree in aerospace engineering from Texas A&M University in 1990. He received an M.S. ('92) and a Ph.D. ('97) in engineering mechanics from the Virginia Polytechnic Institute and State University in Blacksburg, Virginia.

He is a research scientist and program manager in the Composites Branch at the Materials and Manufacturing Directorate, Air Force Research Laboratory (AFRL), Wright-Patterson Air Force Base, Ohio, where he has just completed his 32nd year of employment. His research is focused on experimental mechanics of polymer matrix composites (PMC) and developing digital engineering tools for the processing-to-performance simulation of PMCs and ceramic matrix composites for aerospace.

Dr. Mollenhauer is a member of the American Society for Composites and the American Institute for Aeronautics and Astronautics. He has won numerous technical and program management awards and recently was chosen as an AFRL Fellow.



Craig Przybyla is currently the Research Team Leader of the Composite Performance Team at the Materials and Manufacturing Directorate, Air Force Research Laboratory (AFRL), Wright-Patterson Air Force Base, Ohio where he leads a team of researchers focused on the performance characterization and prediction of advanced polymer and ceramic matrix composites for aerospace applications. His specific area of specialty includes the performance characterization and modeling of composites in

extreme environments. Prior to that assignment, he was a Materials Research Engineer at the Office National d'Etudes et de Recherches Aéronautiques (ONERA) in Châtillon, France as part of the Engineering and Scientist Exchange program between the United States Department of Defense and French Ministry of Defense from 2019-2021. Additional previous assignments include serving the Research Team Leader of the Composites Performance Team between 2015 and 2019 and a Materials Engineer from 2010 to 2014 where he worked as a Research Engineer and subject matter expert for performance characterization and modeling of ceramic matrix composites for hot section components in gas turbine engines and/or thermal protection systems for hypersonic vehicles. Dr. Przybyla first joined the federal civil service in 2007 as a Co-op student in the Metals Branch at AFRL where he developed physics-based performance models to predict fatigue crack initiation in Titanium alloys and Nickel base superalloys. He earned his BS and MS in Mechanical Engineering from Brigham Young University, Provo, Utah in 2004 and 2005, respectively. In 2010, he received his PhD in Materials Science and Engineering at the Georgia Institute of Technology, Atlanta, Ga.



Eann A. Patterson has been the AA Griffith Chair of Structural Materials and Mechanics at the University of Liverpool since 2011 and was appointed Dean of the School of Engineering in 2019. Previously he was Chair of the Department of Mechanical Engineering at Michigan State University and Head of the Department of Mechanical Engineering at the University of Sheffield. His research interests are in experimental mechanics and application of measurement data to support computational modelling in the aerospace, biomedical and energy industries.